JOURNAL OF MATERIALS RESEARCH AND TECHNOLOGY 2021;15:3825–3835

Available online at www.sciencedirect.com

jmr&t Journal of Materials Research and Technology

journal homepage: www.elsevier.com/locate/jmrt

Original Article

# Effect of Ta addition on microstructures, mechanical and damping properties of Cu–Al–Mn–Ti alloy

Liu Yang [a,b], Xiaosong Jiang [a,b,*], Hongliang Sun [a,b], Zhenyi Shao [a,b], Yongjian Fang [c], Rui Shu [d]

[a] Key Laboratory of Advanced Technologies of Materials, Ministry of Education, Chengdu, 610031, China
[b] School of Materials Science and Engineering, Southwest Jiaotong University, Chengdu, Sichuan, 610031, China
[c] School of Mechanical Engineering, Sungkyunkwan University, 2066 Seobu-ro, Jangan-gu, Suwon-si, Gyeonggi-do, 16419, Republic of Korea
[d] Forschungszentrum Jülich GmbH, Institut für Energie-und Klimaforschung Plasmaphysik (IEK-4), Jülich, 52425, Germany

ARTICLE INFO

*Article history:*
Received 8 August 2021
Accepted 6 October 2021
Available online 13 October 2021

*Keywords:*
Spark plasma sintering
Microstructure
Mechanical properties
Damping capacities
Martensite

ABSTRACT

Cu–Al–Mn–Ti–xTa alloys (x = 0, 1, 2, 3, wt.%) prepared by spark plasma sintering were investigated for the effect of Ta content on the microstructure, mechanical and damping properties. The microstructure and phase composition indicate that the alloy is mainly composed of $\beta'_1$ martensite, $\gamma'_1$ martensite, Ti-rich and Ta-rich phase. As the Ta content increases, the grain size of the alloy first decreases and then increases. The reverse trend was observed for hardness, tensile and compressive strength. The hardness, tensile strength and compressive strength increased by 18.2%, 44.9% and 28%, respectively, when the Ta content was 1 wt.% compared to the alloy without Ta element. The presence of martensite provides the alloy with promising damping properties. Meanwhile, the formation of the second phase has a two-sided effect on the damping characteristics. That is, the increase in grain boundaries provides more interfaces for energy dissipation, but the increased compressive stress between the interfaces also hinders the movement of the interfaces. Excellent damping performance is demonstrated with the addition of 1 wt.% of Ta element. The peak values of damping capacity at room temperature and at about 580 °C reached 0.026 and 0.19, respectively. The results confirm that the addition of Ta elements is achievable to obtain Cu–Al–Mn–Ti alloys with both high mechanical and damping properties.



* Corresponding author.
E-mail address: xsjiang@swjtu.edu.cn (X. Jiang).

https://doi.org/10.1016/j.jmrt.2021.10.031

## 1. Introduction

The excellent damping properties provided by the thermoelastic martensite of Cu–Al-based alloys make them become a new functional material with promising applications in mechanical and energy fields [1–3]. However, the large grain size of this system alloy is prone to degraded mechanical properties such as fracture along the grain and low fatigue strength [4–6]. The practical application of damping alloys often requires good mechanical properties as well. Hence, it is necessary to obtain Cu–Al based alloys with high damping and high mechanical properties by controlling the grain size. Alloying is a simple and effective method to adjust the grain size [7–10].

Numerous studies have shown that the addition of the third, fourth and fifth elements can effectively reduce problems such as brittle fracture due to coarse grain size in Cu–Al based alloys [11,12]. Mn elements can broaden the region of the β-phase and reduce its degree of ordering, making Cu–Al–Mn alloys have become another research hotspot [13]. It is shown that the addition of Ce, Ni, Cr, Si, Mg, Fe, and Ti can further improve the properties of Cu–Al–Mn alloy [14]. Among them, the Ti-rich phase formed by the addition of Ti elements can effectively inhibit grain growth and adjust the properties of the alloy [15]. Therefore, it is interesting to study the effect of the fifth element on the Cu–Al–Mn–Ti alloy. So far, the addition of tantalum has shown significant effects on the organization, mechanical properties and phase transition temperatures of other shape memory alloys [16]. And the effect of Ta elements on the damping properties and mechanical properties of Cu–Al–Mn–Ti alloy has not been studied.

Changing sintering process is another method to refine grain size. With the development and demand of functional materials in recent years, it has been shown that spark plasma sintering (SPS) technology can inhibit the grain growth of alloys through rapid sintering [17–19]. What's more, this technology has the advantages of reducing alloy composition segregation, eliminating coarse and inhomogeneous organization, and effectively reducing production energy consumption compared with traditional processes such as melting and casting [17,20,21]. Fang et al. [18] showed that the spark plasma sintering technique plays an important role in optimizing the comprehensive properties of Cu-based alloys by controlling the microstructure.

Therefore, in this paper, Cu–Al–Mn–Ti alloys with different Ta element contents were prepared by spark plasma sintering process from the perspective of adjusting the microstructure. The changes of the microstructure of the alloy were observed, and the mechanism of the effect of Ta elements on the mechanical properties and damping characteristics of Cu–Al–Mn–Ti alloy was discussed in detail.

## 2. Experimental

### 2.1. Materials and preparation of Cu-based alloys

In this experiment, four Cu–11Al–5Mn–0.7Ti–xTa (x = 0,1,2,3, wt.%) alloys were prepared. As the increase of Ta element content, they were numbered as #1, #2, #3 and #4, respectively. The raw materials used were Cu powder, Al powder, Mn powder, Ti powder and Ta powder. First, powders with different contents were added to the planetary ball mill (WL-1) at a ball-to-powder ratio of 7:1, with a ball milling time of 44 h and a ball milling rate of 300 rpm. Tertiary butanol was used as a ball milling medium to reduce oxidation of the powder during ball milling and freeze drying. Then the slurry

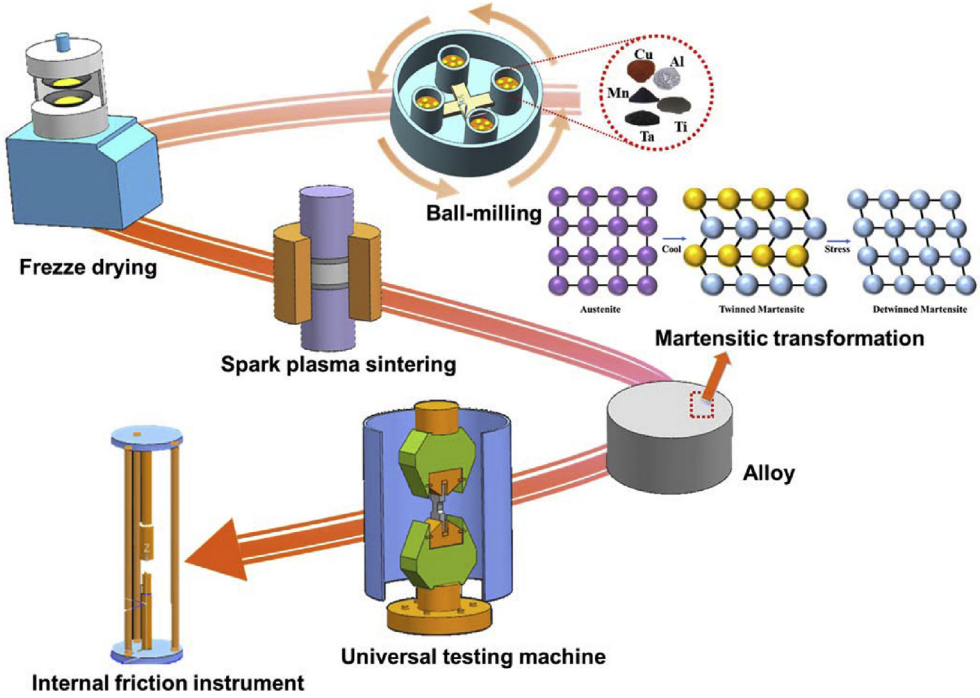


**Fig. 1 – Flow chart of the preparation of Cu–11Al–5Mn–0.7Ti–xTa alloy.**

**Table 1 – Mechanical properties of the alloys.**

| Alloys (wt.%) | Relative density (%) | Hardness (HV) | Tensile strength (MPa) | Compressive strength (MPa) |
|---|---|---|---|---|
| Cu–11Al–5Mn–0.7Ti | 90.6 ± 1.0 | 190.1 ± 9.1 | 266.5 ± 7.9 | 992.1 ± 6.8 |
| Cu–11Al–5Mn–0.7Ti–1Ta | 95.1 ± 0.8 | 233.5 ± 7.2 | 386.1 ± 11.2 | 1269.9 ± 9.2 |
| Cu–11Al–5Mn–0.7Ti–2Ta | 97.5 ± 0.6 | 247.2 ± 12.6 | 393.6 ± 9.3 | 1388.9 ± 7.8 |
| Cu–11Al–5Mn–0.7Ti–3Ta | 92.3 ± 1.6 | 211.9 ± 8.9 | 357.4 ± 8.1 | 1150.8 ± 6.2 |

obtained after ball milling was put into a freeze-drying oven (FD-A-50) for freeze drying, and the desired composite powder was obtained after 24 h of drying. Next, the powder is sintered in an SPS machine (HPD25 from FCT, Germany) to produce a metal block with a diameter of 40 mm and a height of 10 mm. Sintering process parameters: vacuum degree $<10^{-5}$ Pa, heating rate 100 °C/min, heating up to 750 °C, pressurization 40 MPa, holding temperature 10 min and then cool down to 400 °C with the furnace. The experimental flow chart is shown in Fig. 1.

### 2.2. *Characterization of the alloys*

Small squares of size 7 × 7 × 4 mm were cut from the SPS sintered specimens for SEM and XRD. The phase composition of the alloy was determined by X-ray diffraction (XRD, X-Pert) using Cu Kα radiation operated at 40 kV and 20 mA. For the microscopic analyses, the samples were etched with an acid solution of $3HNO_3$:1 HCl:1 $H_2O$. The surface morphology and composition of the specimens were observed by scanning electron microscopy (SEM; JEOL JSM-7001F) coupled with energy dispersive spectroscopy (EDS). Details about the fine microstructure and phase structure were investigated using a Philips CM200 super TWIN (200 kV) transmission electron microscope (TEM) equipped with an EDAX EDX system. The size of TEM specimen is 1 × 1 × 0.1 mm, and then Electron transparent lamellae were prepared by focused ion beam (FIB) standard methods using a FEI Helios NanoLab Dual Beam 650 equipment. The phase transition temperature was determined by differential scanning calorimetry (DSC). The samples were heated from 150 °C to 600 °C at a heating rate of 10 °C/min.

The density of the Alloy was determined by Archimedes drainage method. The hardness was measured with a micro hardness tester (HXD-100TM/LCD) and held for 10 s after loading at 1000 g. The strength was measured with a universal testing machine (WDW-3100) at a speed of 0.5 mm/min, with a tensile strength specimen size of 17 × 2 × 4 mm and a compression strength specimen size of 5 × 5 × 8 mm. After tensile strength measurements, the fracture morphology and elemental composition were characterized. In addition, the room temperature damping and high temperature damping of

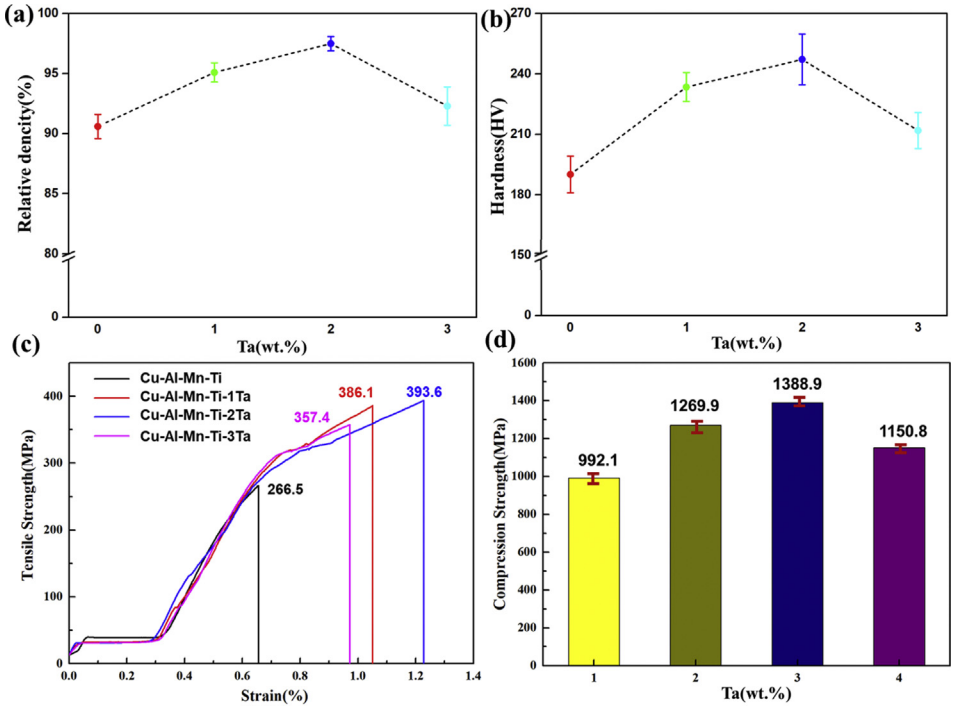


**Fig. 2 – (a) Relative densities of the alloys. (b) Hardness of the alloys. (c) Tensile stress–strain curve of the alloys. (d) Compress strength of the alloys.**

the alloy were tested separately, and the specimen size was 50 × 1.5 × 1.5 mm. The room temperature damping was performed in a multifunctional internal consumption meter (MFP1000) as an inverted torsional pendulum test. The high temperature damping characteristics were characterized by the dynamic mechanics analyzer (TA-Q800). In the single cantilever mode, the test temperature range was room temperature to 600 °C, the frequency was 1 Hz, and the strain amplitude was 1000 × $10^{-6}$.

## 3. Results and discussion

### 3.1. *Mechanical properties of the Cu–Al–Mn–Ti–xTa alloys*

The compactness of the sintered material is an important performance indicator. The density of the material was measured according to Archimedes' principle, and the corresponding relative density was calculated as shown in Table 1. The relative density of Cu–11Al–5Mn–0.7Ti alloy is about 90.6%, and Cu–11Al–5Mn–0.7Ti–2Ta shows the highest relative density of 97.5%. As the contents of Ta increase, the change trend of relative density of the alloy is shown in Fig. 2(a). It can be noticed that the relative density of the alloy shows an overall increasing trend with the addition of Ta content. It was demonstrated that the appropriate Ta element (1 wt.% and 2 wt.% in this study) could prepare high-density Cu–11Al–5Mn–0.7Ti alloys.

The Vickers hardness, tensile and compressive strength of the alloy at room temperature are shown in Table 1. The trends of hardness, tensile and compressive strength with Ta content were displayed in Fig. 2(b)–(d). The mechanical properties of alloys are closely related to their density and microstructure. It can be observed that the trends of hardness, tensile strength and compressive strength are basically the same as the trends of relative density. They all increase as the relative density increases and decrease as the relative density decreases, only with different trends. The hardness, ultimate tensile strength and compressive strength of Cu–11Al–5Mn–0.7Ti alloy are 190.1 HV, 266.5 Mpa and 992.1 Mpa, respectively. The highest hardness, ultimate tensile strength and compressive strengths are 247.2 HV, 393.3 MPa and 1388.9 MPa, respectively, which are shown in the Cu–11Al–5Mn–0.7Ti–2Ta alloy. The effect of microstructure on them will be discussed in later section.

### 3.2. *Damping properties of the Cu–Al–Mn–Ti–xTa alloys*

Fig. 3(a) shows the curves of the damping properties of Cu–Al–Mn–Ti–xTa alloy at room temperature with different amplitudes. The damping properties of all alloys increase with the increase of strain amplitude. Generally, the change in alloy damping is relatively slow at low strain amplitudes. With increasing strain amplitude, the various interfaces of the alloy (phase interfaces, twin surfaces, and metastable interfaces) will be more prone to interfacial movement, consuming more energy and improving the damping performance [22]. In addition, the damping properties of the alloy are also influenced by the Ta element. The damping property of Cu–Al–Mn–Ti alloy is 0.034 and Cu–Al–Mn–Ti–1Ta alloy is 0.026. And the damping decreases with further addition of Ta elements. The change in damping characteristics at room temperature is closely related to the amount of martensite, grain size and second phase distribution. This will be discussed in later sections.

The damping properties and modulus curves of the Cu–Al–Mn–Ti–1Ta alloy during heating are shown in Fig. 3(b). During the heating process a high temperature damping peak appears, which is closely related to the thermoelastic martensitic phase transformation. When the temperature reaches the phase transformation temperature, the amount of phase transformation and the corresponding phase interface increase as the phase transformation proceeds. During the phase transformation process, both the phase transformation product volume effect and the shear motion of different phase interfaces under external alternating stress cause energy loss. When the number of phase interfaces reaches the maximum, the sum of the internal consumption caused by the volume effect of the phase transition and the interfacial viscous motion reaches the maximum, and the peak internal friction of 0.19 occurs at approximately 580 °C. The magnitude of the internal dissipation value during the variable temperature test is obtained from the ratio of the loss modulus to the stored modulus [3]. With a decrease in storage modulus, the damping increases and the maximum damping appears at the lowest storage modulus, which is consistent with Fig. 3(b).

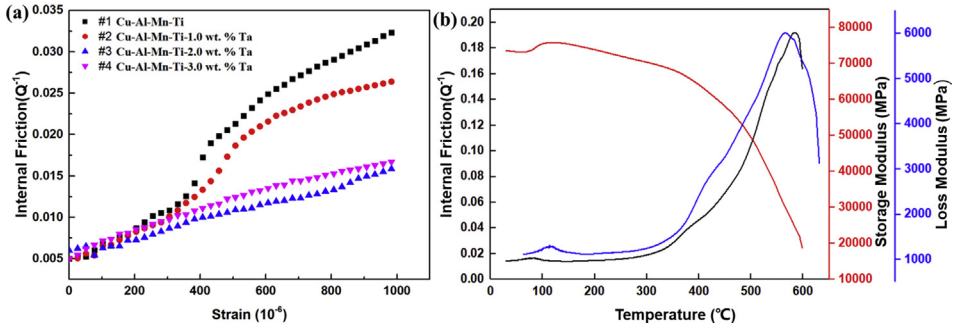


**Fig. 3 – (a) Damping properties of Cu–11Al–5Mn–0.7Ti–xTa alloy at room temperature. (b) Damping properties and modulus curves of Cu–Al–Mn–Ti–1Ta alloy during heating.**

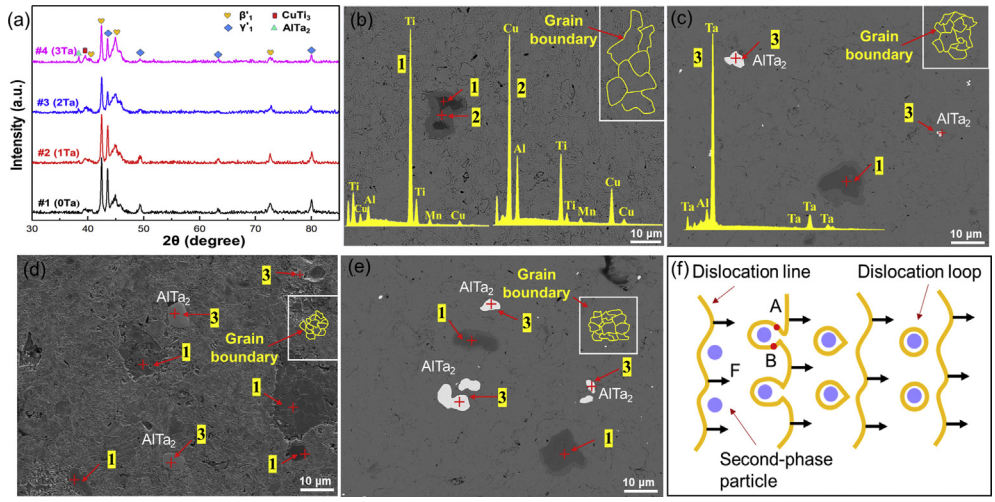


**Fig. 4 – (a) XRD pattern of Cu–11Al–5Mn–0.7Ti–xTa with different Ta contents. (b–e) BSE morphology of Cu–11Al–5Mn–0.7Ti–xTa alloys. Cu–11Al–5Mn–0.7Ti, Cu–11Al–5Mn–0.7Ti–1Ta, Cu–11Al–5Mn–0.7Ti–2Ta, Cu–11Al–5Mn–0.7Ti–3Ta, respectively. (f) Dispersion strengthening mechanism.**

### 3.3. *Characterization of the Cu–Al–Mn–Ti–xTa alloys*

In order to analyze the mechanism of the influence of Ta elements, extensive microscopic characterization of Cu–Al–Mn–Ti alloy was carried out. The XRD patterns of the Cu–Al–Mn–Ti alloy with different Ta elements are shown in Fig. 4(a). The alloy is mainly composed of $\beta'_1$ martensite, $\gamma'_1$ martensite and $CuTi_3$. The new phase $AlTa_2$ is accompanied by the addition of Ta elements. The peak intensity of $AiTa_2$ was enhanced with increasing Ta content. Martensite is formed during the rapid cooling process when using SPS sintering. They have close chemical composition and inherit the ordered arrangement of the parent phase and become thermoelastic martensite [23,24]. Meanwhile, according to the height shift of the strongest peak of $\beta'_1$ and $\gamma'_1$, the height continues to decrease with the addition of 1 wt.% and 2 wt.% Ta elements. However, the height increases after the addition of 3 wt.% Ta element compared to 2 wt.% Ta. The variation of martensite strength has the same trend as Fig. 3(a). It is shown that the Ta element can change the damping properties of the alloy by affecting the amount of martensite. For the Cu–Al–Mn–Ti alloy, its damping properties are mainly derived from its inherent thermoelastic martensite. Usually, the increase in the number and type of martensite provides more interfaces for energy consumption and obtains higher damping properties [23].

Fig. 4(b)–(e) shows the BSE morphology with different contents of Ta element, and the different precipitated phases were tested using EDS spectroscopy. In Fig. 4(b), the main precipitated phase is the Ti-rich phase for the alloy without the addition of Ta element. The EDS results show that the contrast between the two regions is different due to the different contents of Ti element at point 1 (85.2 at.%) and point 2 (25.2 at.%). In general, the microstructure contrast is correlated with the atomic number in the SEM backscattering mode [25]. Point 1 has more Ti content compared to point 2, indicating that the point 1 region is mainly an aggregation zone of Ti-rich phase. In addition, according to the energy spectrum analysis, Ta-rich phase ($AlTa_2$) appeared after addition of Ta, which is consistent with the XRD results. The formation of this phase is mainly due to the different crystal structures of Al (FCC) and Ta atomic (BCC), which are almost insoluble in the solid state [26]. In addition, the atomic radius of Ta and Ti atoms is larger than that of Cu, Al, and Mn atoms, which makes Ta and Ti atoms less soluble in the substrate and thus forms the second phase.

In addition to changing the martensite content, the Ta element can also affect the damping properties of the alloy by adjusting the grain size. In order to show the grain size change more clearly, the local grain boundaries, which represent the overall grain size change trend, are darkened in the figure, as shown in Fig. 4(b)–(e). Without Ta elements, the damping peak reaches 0.034; after adding 1 wt.% of Ta elements, the damping peak decreases to nearly 0.026, as shown in Fig. 3(a). This is due to the decrease in grain size, which increases the compressive stress at the near-neighbor interface as well as the elevated bonding forces at the grain boundaries, leading to a decrease in interfacial slip [27]. When 2 wt.% Ta is added, the damping properties of the alloy decrease sharply. This is mainly caused by the greater interfacial binding force produced by the reduced grain size. Moreover, the suppression of interfacial mobility by the second phase particles outweighs the damped interfacial effect of the increased second phase. The Cu–Al–Mn–Ti–3Ta alloy shows a slight increase in damping, which is related to a slight increase in grain size. In conclusion, the element Ta can influence the damping properties by affecting the amount of martensite and the grain size in the alloy.

Moreover, the formation of the second phase leads to fine grain strengthening and dispersion strengthening that can also affect the mechanical properties of the alloy. It can be found that the grain size decreases first with the addition of Ta elements. This is attributed to the pinning effect of the second to grain boundary [28,29]. When 3 wt.% Ta was added, an abnormal growth of grains occurred. This may be due to the formation of an oversized and unevenly distributed $AlTa_2$

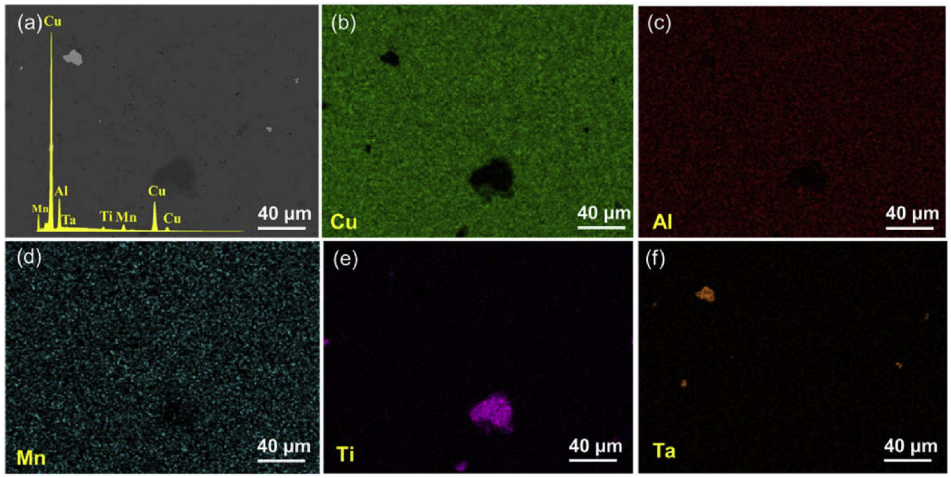


**Fig. 5 – (a) SEM image of the Cu–11Al–5Mn–0.7Ti–1Ta alloy. (b–f) Distribution of different elements on the surface.**

phase, causing some grain boundaries to be completely pinned and others to be completely unpinned. The unpinned grain boundaries evolve quickly and will merge with the surrounding grains, leading to anomalous grain growth. After grain refinement, the number of grain boundaries increases, which expands the dislocation blockage and increases the strength of the alloy; when the grains grow, the obstruction of dislocation movement by grain boundaries decreases and the strength reduces, which is consistent with the results of Fig. 2(c) and (d).

Fig. 4(f) shows the dispersion strengthening effect played by the generated second phase $AlTa_2$. It is mainly achieved through the interaction of second-phase particles with dislocations. The dislocation line is blocked by the second phase particle during its motion. And the increase of the applied shear stress bends the dislocations until they meet at A and B.

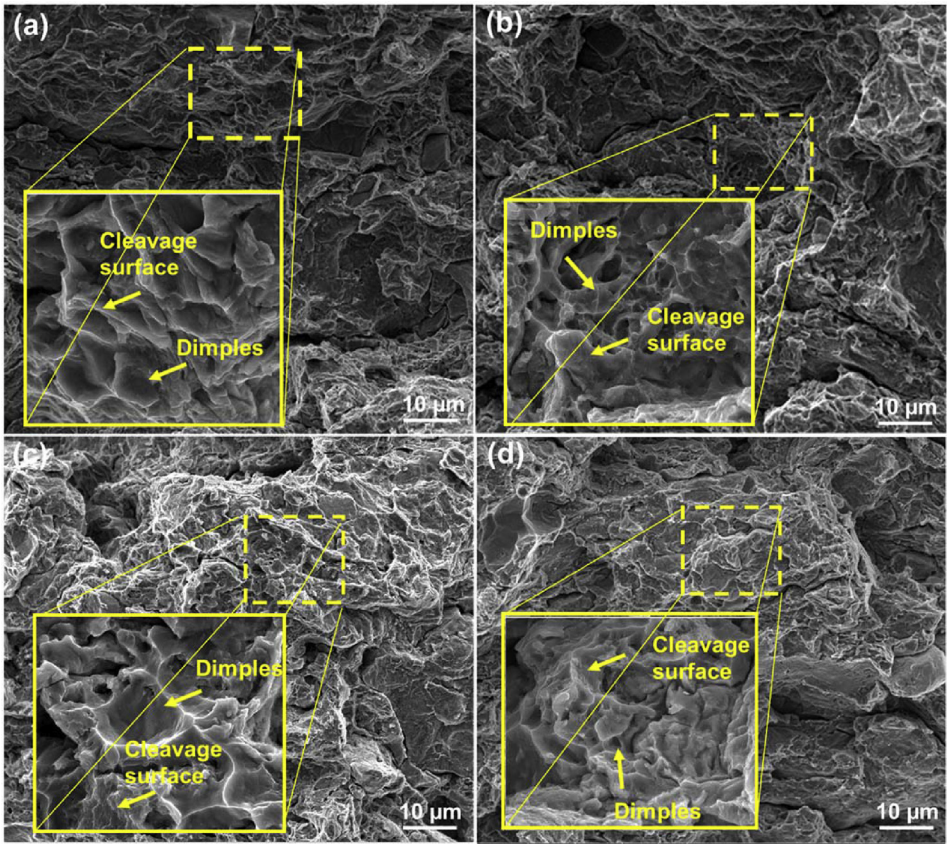


**Fig. 6 – SEM micrograph of fracture surface. (a) Cu–11Al–5Mn–0.7Ti. (b) Cu–11Al–5Mn–0.7Ti–1Ta. (c) Cu–11Al–5Mn–0.7Ti–2Ta. (d) Cu–11Al–5Mn–0.7Ti–3Ta.**

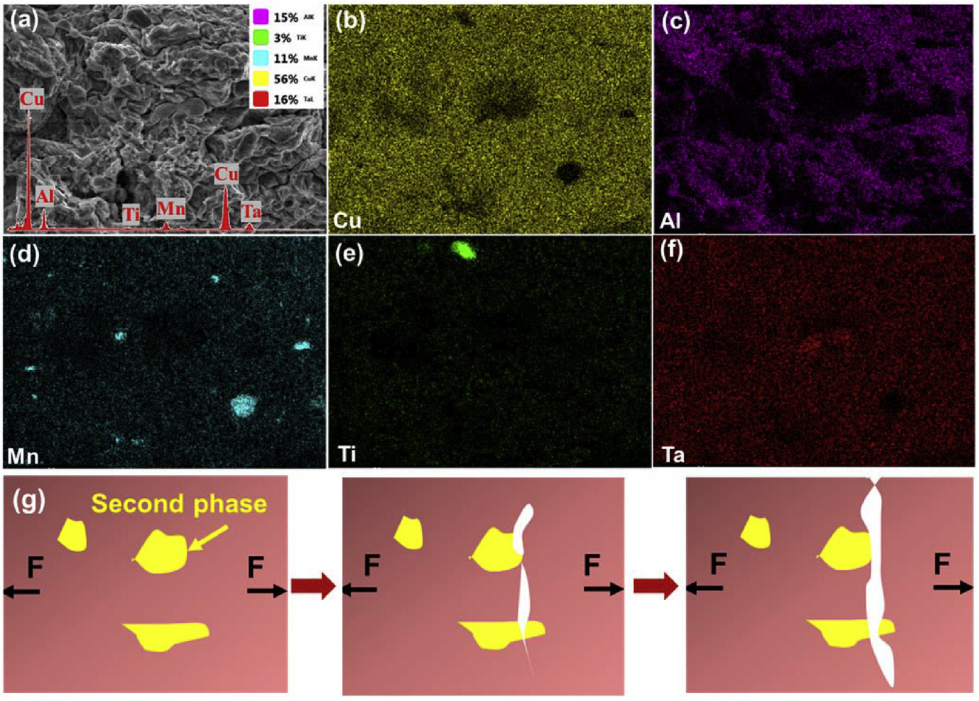


**Fig. 7 – (a) SEM image of the fracture morphology. (b–f) EDS surface scanning diagram of fracture surface. (g) Schematic diagram of the effect of second phase on tensile fracture.**

Then, the dislocation lines A and B in opposite directions meet and cancel, leaving a dislocation loop. Subsequently, the dislocation lines bypass the particles and return to their original state and continue sliding. The combined effect of this process and grain refinement increases the strength of the alloy.

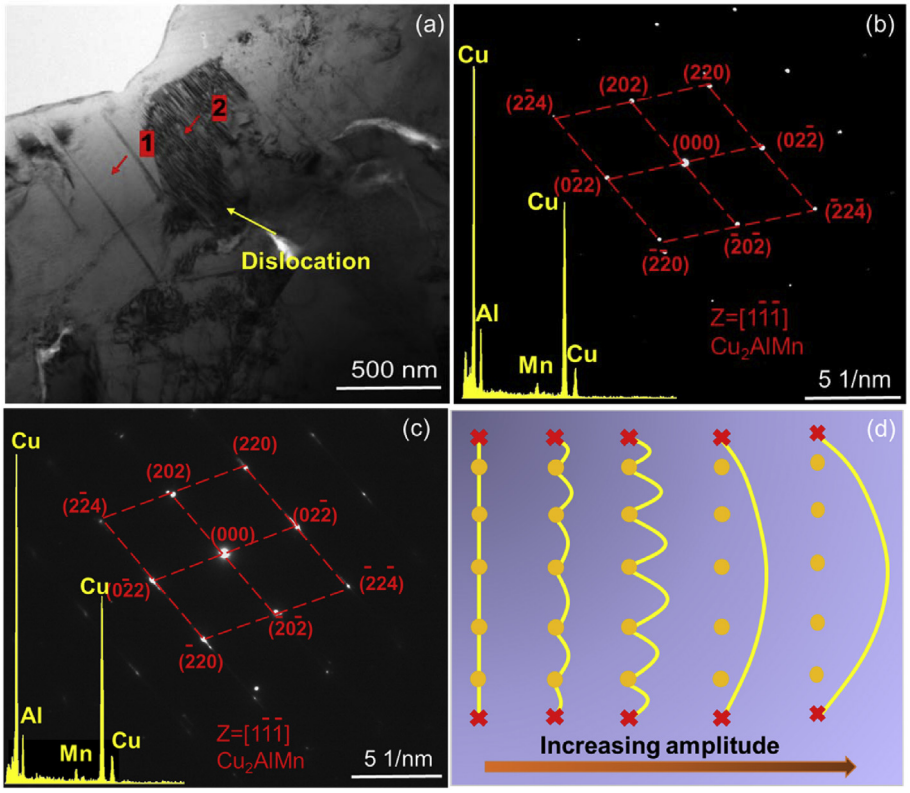


**Fig. 8 – (a) TEM bright-field images of Cu–11Al–5Mn–0.7Ti–1Ta alloy. (b–c) Corresponding to the electron diffraction patterns of regions 1 and 2 in Fig. (a), respectively. (d) Dislocation damping pinning model.**

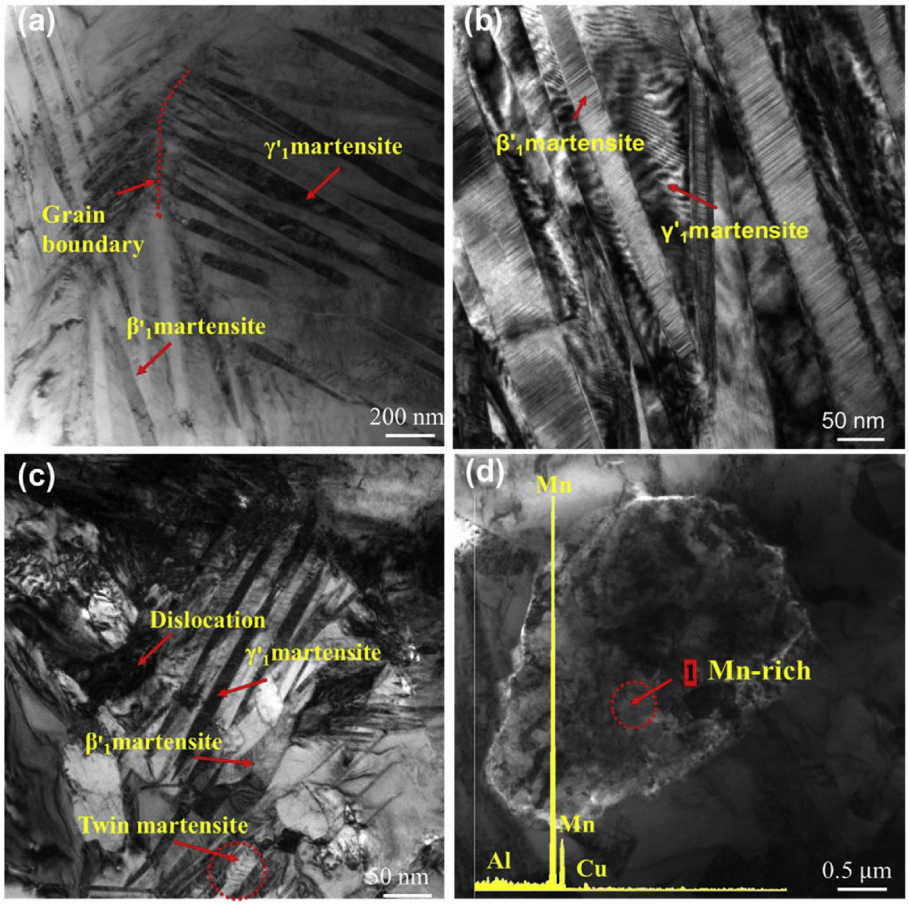


**Fig. 9 – (a–c) TEM bright-field images of the martensitic structure of different regions of Cu–11Al–5Mn–0.7Ti–1Ta alloy. (d) TEM bright field images of the Mn-rich phase.**

The surface SEM morphology of Cu–11Al–5Mn–0.7Ti–1Ta is shown in Fig. 5. It is observed that the overall distribution of the elements is relatively uniform and no obvious holes appear. Moreover, the Ti-rich and Ta-rich phases are mainly precipitated, which is consistent with the results in Fig. 4. This indicates the superiority of SPS sintering in obtaining highly dense materials, which is consistent with the high densities shown by the materials in Table 1.

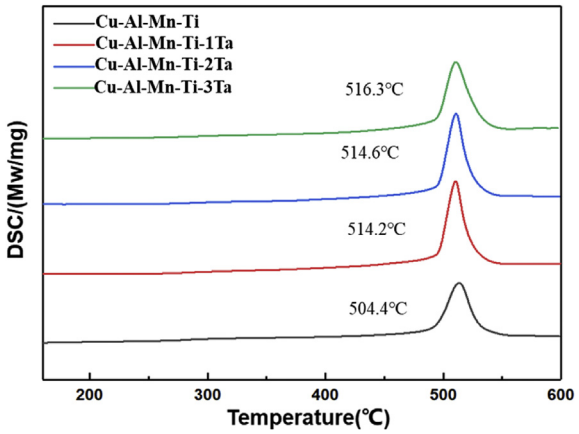


**Fig. 10 – DSC curves of the Cu–11Al–5Mn–0.7Ti–xTa alloys with different Ta contents.**

Fig. 6 shows the SEM morphology of the tensile fracture of the Cu–11Al–5Mn–0.7Ti–xTa alloy. The solid yellow areas (in the web version) for each group of specimens are enlarged areas with yellow dashed boxes. From the dimples and cleavage surfaces, which are present in each group of fractures, it can be inferred that the alloy is a mixture of ductile and brittle fractures. The Cu–11Al–5Mn–0.7Ti–2Ta alloy has the largest number and depth of dimples and shows the best strength, which is consistent with Fig. 2(c). The number of toughness dimples decreases with further addition of Ta elements, the alloy is prone to fracture and the tensile strength decreases.

The fracture surface of Cu–11Al–5Mn–0.7Ti–2Ta alloy are shown in Fig. 7(a)–(f). It shows that the elemental distribution is not uniform throughout the fracture, and second phase aggregation of Mn, Ti, and Ta elements occurs. The second phase can affect the mechanical and damping properties of the alloy by changing the grain size and the number of grain boundaries, as mentioned in the previous analysis. Fig. 7(g) shows the schematic diagram of tensile fracture after the addition of alloying elements. Where the direction perpendicular to the stress is more likely to form a crack source and thus fracture. Depending on the shape size dimensions of the second phase, fracture is more likely to occur near the larger second phase [30]. A properly sized second phase can effectively prevent crack propagation or change the direction of crack propagation. Thus, it is again evident that the mechanical properties of

the alloy were improved by the appropriate addition of the appropriate content of Ta elements in this experiment.

To further analyze the microstructure of the samples, TEM tests were performed on the Cu–11Al–5Mn–0.7Ti–1Ta alloy, and the results are shown in Fig. 8(a)–(c). The energy spectrum results show the same composition in both regions 1 and 2. Combined with the results of the electron diffraction region, they are both $Cu_2AlMn$. In addition, the appearance of dislocation structures in region 2 is usually closely related to the damping properties of the alloy with different amplitudes. The dislocation-damped pinning model is shown in Fig. 8(d). Usually, the dislocations are pinned by the second-phase particles; as the strain amplitude increases, the dislocations protrude into an arc; after the strain amplitude increases further, the dislocations can break away from the weak pinned points of the second-phase particles and restrain themselves to the strong pinned points, forming a dislocation ring. This process consumes energy and increases the damping properties [31], which corresponds to Fig. 3(a).

Fig. 9 shows the TEM bright-field images of different regions of the Cu–11Al–5Mn–0.7Ti–1Ta alloy. In Fig. 9(a), two different β′1 and γ′1 martensitic laths can be observed separated from each other by grain boundaries. In Fig. 9(b) it is observed that the substructure of β′1 martensite is lamellar dislocation and the substructure of γ′1 martensite is twinning. Generally, γ′1 martensite has many mobile twin structures, which are highly mobile and favor the energy consumption of the alloy and increase the damping properties [23]. The β′1 martensite also promotes the damping properties of the alloy because its growth in the adaptive group is controlled [22]. In addition to the different martensitic variants observed, localized dislocation regions are also present, as shown in Fig. 9(c). The main source of damping in copper-based alloys is the hysteretic mobility of the various phase interfaces and twin grain boundaries in the martensitic variant [32]. During the thermoelastic martensitic phase transformation, different martensitic variants can reduce the stresses formed during the phase transformation and the stored elastic modulus, which favors the damping capacity of the alloy, becomes "self-regulation" [31]. And, a phase transition damping peak appears during the heating or cooling process, indicating that the interpretation of Fig. 3(b) is correct. Fig. 9(d) shows the presence of a Mn-rich phase, which is not observed in both XRD and SEM, probably due to this phase is only present in tiny amounts in localized areas.

The DSC curves of Cu–Al–Mn–Ti–xTa alloys during heating are shown in Fig. 10. As the temperature increases, a phase transformation peak gradually appears at the beginning of the smoothing curve, which is consistent with the value of the variable temperature damping peak in Fig. 3(b). It shows that the alloy has a martensitic structure that provides damping properties by undergoing phase transformation during the heating process. The difference between the temperature of the DSC curve peak and the temperature of the variable temperature damping peak may be due to the small differences that occur in different parts of the alloy and the different sensitivity of the different equipment during the test. In addition, as the Ta element increases, the phase transition temperature of the alloy shift to high temperature side. This requires consideration of the changes to the Al element in the alloy with the addition of the Ta element. According to the Cu–Al binary phase diagram, the decrease of Al content will increase the phase transition temperature. According to Fig. 4(b)–(e), the amount of $AlTa_2$ increases with the increase of Ta content. The increase of $AlTa_2$ phase decreases the Al content in the substrate and thus increases the phase transition temperature. Combining the phase transition temperature in Fig. 10 and the high temperature damping peak appearing in Fig. 3(b), it can be inferred that this experiment achieves higher temperature damping applications compared to the existing Cu–Al based alloys.

## 4. Conclusion

In this paper, Cu–11Al–5Mn–0.7Ti alloys with different Ta contents were successfully prepared by spark plasma sintering technique. The effects of Ta content on the microstructure, mechanical properties and damping properties of Cu–Al–Mn–Ti alloys were investigated. The conclusions are as follows:

1. The ultimate tensile strength, compressive strength and room temperature damping properties of the alloy reached 386.1 MPa, 1269.9 MP and 0.026, respectively, when only 1 wt.% of Ta element was added, although the damping properties decreased to some extent compared to those without the addition of Ta element. It is shown that the alloy with both high mechanical and damping properties can be obtained by adding appropriate content of Ta elements to Cu–Al–Mn–Ti-based alloys.
2. The improvement of the mechanical properties is mainly achieved by the combined effect of fine grain strengthening and second phase dispersion strengthening after the addition of Ta elements.
3. The change in room temperature damping properties of the alloy after the addition of Ta is attributed to the combined effect of the change in grain size, martensite amount and the dislocation damping effect. And the grain refinement has a two-sided effect on the damping properties of the alloy. On the one hand, more movable interfaces can be added to consume energy; on the other hand, the increased compressive stress between the interfaces can hinder the movement of the interfaces.
4. The energy absorbed by the migration of β′1 martensite and γ′1 martensite as well as various interfaces (phase interfaces, twin surfaces, and metastable interfaces) facilitates room-temperature damping. In addition, attractive high-temperature damping can also be achieved by phase transformation of martensite during heating. The damping in this experiment reached 0.19 at about 580 °C, which provides a reference for higher temperature damping applications of Cu–Al based alloys.

## Data availability statement

The data used to support the findings of this study are available from the corresponding author upon request.

## Declaration of Competing Interest

The authors declare that they have no known competing financial interests or personal relationships that could have appeared to influence the work reported in this paper.

## Acknowledgments

This work was supported by Key Laboratory of Infrared Imaging Materials and Detectors, Shanghai Institute of Technical Physics, Chinese Academy of Sciences (No. IIMDKFJJ-19-08), China Postdoctoral Science Foundation (No. 2015M570794, No. 2018T110993).

## REFERENCES

[1] Vajpai SK, Dube RK, Sangal S. Microstructure and properties of Cu-Al-Ni shape memory alloy strips prepared via hot densification rolling of argon atomized powder preforms. Mater Sci Eng A 2011;529:378–87. https://doi.org/10.1016/j.msea.2011.09.046.

[2] Fu H, Xu S, Zhao H, Dong H, Xie J. Cyclic stress-strain response of directionally solidified polycrystalline Cu-Al-Ni shape memory alloys. J Alloy Compd 2017;714:154–9. https://doi.org/10.1016/j.jallcom.2017.04.234.

[3] Laper ML, Guimaraes R, Barrioni BR, Silva PAP, Houmard M, Mazzer EM, et al. Fabrication of porous samples from a high-temperature Cu-Al-Ni-Mn-Nb shape memory alloy by freeze-drying and partial sintering. J Mater Res Technol 2020;9(3):3676–85. https://doi.org/10.1016/j.jmrt.2020.01.105.

[4] Karagoz Z, Canbay CA. Relationship between transformation temperatures and alloying elements in Cu-Al-Ni shape memory alloys. J Therm Anal Calorim 2013;114(3):1069–74. https://doi.org/10.1007/s10973-013-3145-9.

[5] Sutou Y, Omori T, Kainuma R, Ono N, Ishida K. Enhancement of superelasticity in Cu-Al-Mn-Ni shape-memory alloys by texture control. Metall Mater Trans A 2002;33(9):2817–24. https://doi.org/10.1007/s11661-002-0267-2.

[6] Grguric TH, Manasijevic D, Kozuh S, Ivanic I, Anzel I, Kosec B, et al. The effect of the processing parameters on the martensitic transformation of Cu-Al-Mn shape memory alloy. J Alloy Compd 2018;765:664–76. https://doi.org/10.1016/j.jallcom.2018.06.250.

[7] Sari U. Influences of 2.5wt% Mn addition on the microstructure and mechanical properties of Cu-Al-Ni shape memory alloys. Int J Miner Metall Mater 2010;17(2):192–8. https://doi.org/10.1007/s12613-010-0212-0.

[8] Mazzer EM, Kiminami C, Bolfarini C, Cava RD, Botta WJ, Gargarella P. Thermodynamic analysis of the effect of annealing on the thermal stability of a Cu-Al-Ni-Mn shape memory alloy. Thermochim Acta 2015;608:1–6. https://doi.org/10.1016/j.tca.2015.03.024.

[9] Li D, Zhang S, Liao W, Geng G, Zhang Y. Superelasticity of Cu-Ni-Al shape-memory fibers prepared by melt extraction technique. Int J Miner Metall Mater 2016;23(8):928–33. https://doi.org/10.1007/s12613-016-1308-y.

[10] Yildiz K. Effect of aging on structure and shape memory behavior of a Cu-Al-Mn-Ti-C shape memory alloy. Thermochim Acta 2020;693:178760. https://doi.org/10.1016/j.tca.2020.178760.

[11] Perez-Landazabal JI, Recarte V, Sanches-Alarcos V, Nó ML, Juan JS. Study of the stability and decomposition process of the β phase in Cu-Al-Ni shape memory alloys. Mater Sci Eng A 2006;438:734–7. https://doi.org/10.1016/j.msea.2005.12.066.

[12] Sutou Y, Omori T, Yamauchi K, Ono N, Kainuma R, Ishida K. Effect of grain size and texture on pseudoelasticity in Cu-Al-Mn-based shape memory wire. Acta Mater 2005;53(15):4121–33. https://doi.org/10.1016/j.actamat.2005.05.013.

[13] Lu X, Chen F, Li W, Zheng Y. Effect of Ce addition on the microstructure and damping properties of Cu-Al-Mn shape memory alloys. J Alloy Compd 2009;480(2):608–11. https://doi.org/10.1016/j.jallcom.2009.01.134.

[14] Manasijevic D, Grguric TH, Balanovic L, Stamenkovic U, Gorgievski M, Gojic M. Effect of Mn content on the microstructure and phase transformation temperatures of the Cu-Al-Mn-Ag shape memory alloys. Kov Mater 2020;58:293–9. https://doi.org/10.4149/km_2020_4_293.

[15] Dalvand P, Raygan S, Lopez GA, Melendez MB, Chernenko VA. Properties of rare earth added Cu-12wt%Al-3wt%Ni-0.6wt%Ti high temperature shape memory alloy. Mater Sci Eng A 2019;754:370–81. https://doi.org/10.1016/j.msea.2019.03.022.

[16] Saud SN, Hamzah E, Bakhsheshi-Rad HR, Abubakar T. Effect of Ta additions on the microstructure, damping, and shape memory behaviour of prealloyed Cu-Al-Ni shape memory alloys. Scanning 2017;2017:1–13. https://doi.org/10.1155/2017/1789454.

[17] Eze AA, Jamiru T, Sadiku ER, Durowoju MO, Kupolati WK, Ibrahim ID, et al. Effect of titanium addition on the microstructure, electrical conductivity and mechanical properties of copper by using SPS for the preparation of Cu-Ti alloys. J Alloy Compd 2018;736:163–71. https://doi.org/10.1016/j.jallcom.2017.11.129.

[18] Fang Q, Kang Z, Gan Y, Long Y. Microstructures and mechanical properties of spark plasma sintered Cu-Cr composites prepared by mechanical milling and alloying. Mater Des 2015;88:8–15. https://doi.org/10.1016/j.matdes.2015.08.127.

[19] Dash K, Ray BC, Chaira D. Synthesis and characterization of copper-alumina metal matrix composite by conventional and spark plasma sintering. J Alloy Compd 2012;516:78–84. https://doi.org/10.1016/j.jallcom.2011.11.136.

[20] Zhang M, Liu K, Han J, Qian F, Wang J, Guan S. Investigating the role of Cu, Zr and V on the evolution of microstructure and properties of Al-Si-Mg cast alloys. Mater Today Commun 2021;26:102055. https://doi.org/10.1016/j.mtcomm.2021.102055.

[21] Hungria T, Galy J, Castro A. Spark plasma sintering as a useful technique to the nanostructuration of piezo-ferroelectric materials. Adv Eng Mater 2009;11(8):615–31. https://doi.org/10.1002/adem.200900052.

[22] Sari U, Aksoy H. Electron microscopy study of 2H and 18R martensites in Cu-11.92 wt% A1-3.78 wt% Ni shape memory alloy. J Alloy Compd 2006;417(1–2):138–42. https://doi.org/10.1016/j.jallcom.2005.09.049.

[23] Portier RA, Ochin P, Pasko A, Monastyrsky GE, Gilchuk AV, Kolomytsev VI, et al. Spark plasma sintering of Cu-Al-Ni shape memory alloy. J Alloy Compd 2013;577:S472–7. https://doi.org/10.1016/j.jallcom.2012.02.145.

[24] Samal P, Vundavilli PR, Meher A, Mahapatra MM. Recent progress in aluminum metal matrix composites: a review on processing, mechanical and wear properties. J Manuf Process 2020;59:131–52. https://doi.org/10.1016/j.jmapro.2020.09.010.

[25] Yang L, Jiang X, Sun H, Song T, Mo D, Li X, et al. Interfacial reaction and microstructure investigation of TC4/V/Cu/Co/316L diffusion-bonded joints. Mater Lett 2020;261:127140. https://doi.org/10.1016/j.matlet.2019.127140.

[26] Pun GPP, Darling KA, Kecskes LJ, Mishin Y. Angular-dependent interatomic potential for the Cu-Ta system and

its application to structural stability of nano-crystalline alloys. Acta Mater 2015;100:377–91. https://doi.org/10.1016/j.actamat.2015.08.052.

[27] Saud SN, Hamzah E, Abubakar T, Ibrahim MK, Bahador A. Effect of a fourth alloying element on the microstructure and mechanical properties of Cu-Al-Ni shape memory alloys. J Mater Res 2015;30(14):2258–69. https://doi.org/10.1557/jmr.2015.196.

[28] Saud SN, Hamzah E, Abubakar T, Zamri M, Tanemura M. Influence of Ti additions on the martensitic phase transformation and mechanical properties of Cu-Al-Ni shape memory alloys. J Therm Anal Calorim 2014;118(1):111–22. https://doi.org/10.1007/s10973-014-3953-6.

[29] Ding Y, Wang Q, Yin F, Cui C, Hao G. Effect of combined addition of Cu51Zr14 inoculant and Ti element on the microstructure and damping behavior of a Cu-Al-Ni shape memory alloy. Mater Sci Eng A 2019;743:606–10. https://doi.org/10.1016/j.msea.2018.11.124.

[30] Lopez-Ferreno I, Gomez-Cortes JF, Breczewski T, Ruiz-Larrea I, No ML, San J, et al. High-temperature shape memory alloys based on the Cu-Al-Ni system: design and thermomechanical characterization. J Mater Res Technol 2020;9(5):9972–84. https://doi.org/10.1016/j.jmrt.2020.07.002.

[31] Chang S, Liao B, Gholami-Kermanshahi M. Effect of Co additions on the damping properties of Cu-Al-Ni shape memory alloys. J Alloy Compd 2020;847:156560. https://doi.org/10.1016/j.jallcom.2020.156560.

[32] Sampath V. Studies on the effect of grain refinement and thermal processing on shape memory characteristics of Cu-Al-Ni alloys. Smart Mater Struct 2005;14(5):S253–60. https://doi.org/10.1088/0964-1726/14/5/013.